# Appendix A

## Composition and density of Tail gas

### A.1 Composition of tail gas

Table A.1 given the composition of tail gas as measured at SSF with molecular weight of 17.9 kg/kmol.

Table A.1: Composition of tail gas

| | Volume % |
|---|---|
| $CO_2$ | 11.7 |
| $C_2H_4$ | 2.15 |
| $C_2H_6$ | 0.913 |
| $H_2$ | 36.31 |
| $CH_4$ | 37.55 |
| CO | 1.049 |
| $C_3H_6$ | 3.3 |
| $C_3H_8$ | 1.8 |
| i-$C_4H_{10}$ | 2.2 |
| n-$C_4H_{10}$ | 1 |
| $C_4H_8$ | 0.6 |
| cis-$C_4H_8$ | 1.4 |

### A.2 Density of tail gas

The equation of state for gases at low density is given by the following equation (Van Wylen *et al.* 1993):

$$P\bar{v} = \bar{R}T \qquad \text{A.1}$$

Equation A.1 can be written in terms of the total volume:

$$PV = mRT \qquad \text{A.2}$$

$R$ is the gas constant for the particular gas, and can be calculated as follows:

$$R = \frac{\overline{R}}{M} \qquad \text{A.3}$$

By substituting $\overline{R}$, the universal gas constant (8.3145 kN m/kmol K) and M, the molecular weight of tail gas (17.9 kg/kmol) into equation A.3, a gas constant of 0.464497 kN m/kmol K is obtained.

### A.2.1 Normal conditions

The measured flow rates through the heat exchanger were measured at normal conditions (101 kPa and 273 K). If the pressure and temperature are substituted into equation A.2, a density of 0.796 kg/m$^3$ is obtained.

### A.2.1 Operating conditions

By substituting the inlet temperature (328K) and pressure (3225 kPa) into equation A.2, a density of 21 kg/m$^3$ is obtained.

# Appendix B

## Flow velocity calculations

### B. 1 Flow velocity calculations

The flow velocity through the heat exchanger was altered by first opening the bypass valve in 100 mm increments and then closing the heat exchanger valve also in increments of 100 mm. The losses in both the loops were calculated as follows:

### B.1.1 Bypass loop

The total pipe length is 15.81 m with three 90° elbow fittings, one 24" gate valve, one branch flow tee and one line flow tee. The average loss coefficient K for the gate valve as a function of the fractional opening is given in figure B.1.

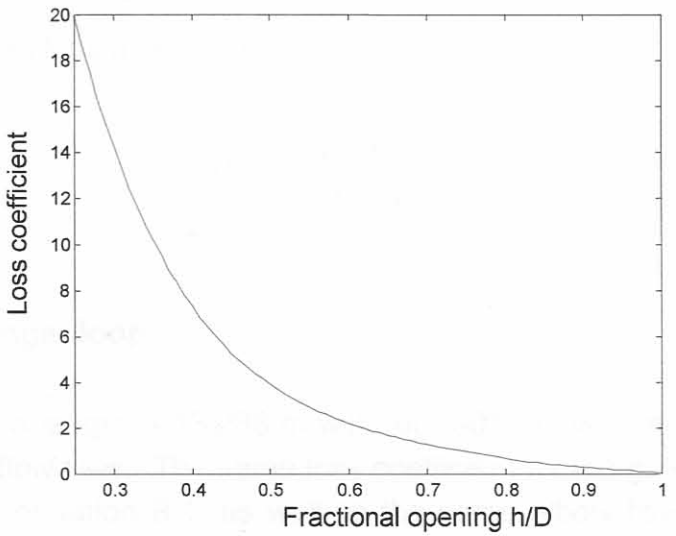


*Figure B.1: Average loss coefficient for partially open gate valves (White, 1994)*

Loss coefficient data from White (1994) was used to fit a $5^{th}$ order polynomial curve:

$$K_{gv} = -2.061\times10^{2}\left(\frac{h}{D}\right)^{5} + 8.533\times10^{2}\left(\frac{h}{D}\right)^{4} - 1.414\times10^{3}\left(\frac{h}{D}\right)^{3} + 1.183\times10^{3}\left(\frac{h}{D}\right)^{2} - 5.077\times10^{2}\left(\frac{h}{D}\right)^{1} + 91.86 \quad \text{B.1}$$

The 90° elbow fitting loss coefficient was calculated as 0.25, the line flow tee loss coefficient as 0.07 and the branch flow tee loss coefficient as 0.41, using data from White (1994).

This gives a total loss coefficient $K_t$ of:

$$K_t = 1.23 + K_{gv} \quad \text{B.2}$$

The friction factor ($f$) was calculated using an explicit formula given by Haaland (1983) as

$$\frac{1}{f^{\frac{1}{2}}} \approx -1.8\log\left[\frac{6.9}{\mathrm{Re}_d} + \left(\frac{\frac{\varepsilon}{d}}{3.7}\right)^{1.11}\right] \quad \text{B.3}$$

The total head loss across the bypass is:

$$\Delta h_{bp} = \frac{V_{bp}}{2g}\left(\frac{f_{bp}L_{bp}}{d_{bp}} + K_t\right) \quad \text{B.4}$$

### B.1.2 Heat exchanger loop

The total pipe length is 13.288 m with four 90° elbow fittings, one 24" gate valve, two branch flow tees. The same loss coefficient for the gate valve was used as in fig. B.1 and equation B.1, as well as the same elbow fitting loss coefficient and branch flow tee loss coefficient.

This gives a total loss coefficient of:

$$K_t = 1.82 + K_{gv} \quad \text{B.5}$$

Equation B.3 was used to calculate the friction factor (*f*).

The pressure drop across the heat exchanger is a function of the mass flow rate. A curve was fitted through the HTRI pressure values (see figure B.3 and equation B.6), using Matlab's `polyfit` function.

$$\Delta P = 7.828\times10^{-3}\dot{m}^2 + 7.008\times10^{-2}\dot{m} - 3.787\times10^{-1} \qquad \text{B.6}$$

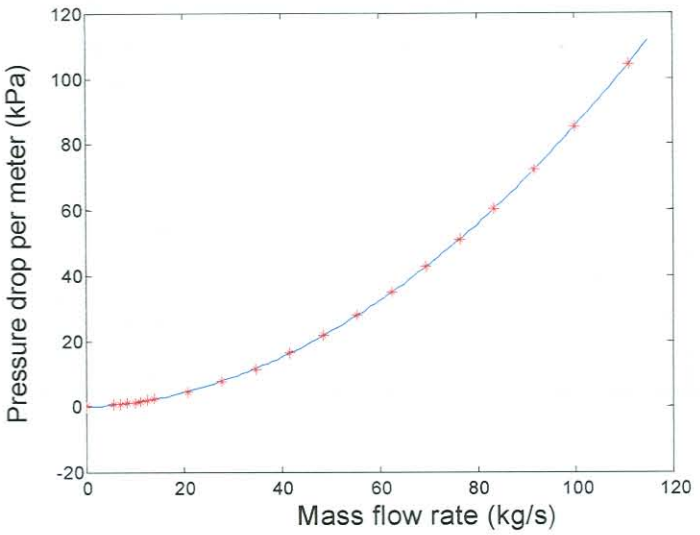


*Figure B.2: Pressure drop per meter across the heat exchanger*

The total head loss across the heat exchanger loop is:

$$\Delta h_{he} = \frac{V_{he}}{2g}\left(\frac{f_{he}L_{he}}{d_{he}} + K_t\right) + \frac{\Delta p_{he}}{\rho g} \qquad \text{B.7}$$

The heat exchanger and bypass loop is in parallel and therefore the loss is the same in each loop. By solving equation B.8 with Matlab's `fsolve` function, the flow velocities through the heat exchanger were calculated as shown in Table B.1.

$$\Delta h_{he} - \Delta h_{bp} = 0 \qquad \text{B.8}$$

Table B.1 Velocities associated with measuring sets

| Set | Bypass valve pos. | Heat Exc. valve pos. | Total velocity | Bypass velocity | Heat Exc. velocity |
|---|---|---|---|---|---|
| 1 | Closed | open | 14.77972 | 0.00000 | 14.77972 |
| 2 | 100mm | open | 14.78307 | 11.29579 | 3.48728 |
| 3 | 200mm | open | 14.8547 | 12.74159 | 2.11311 |
| 4 | 300mm | open | 14.92133 | 13.51935 | 1.40198 |
| 5 | 400mm | open | 15.09434 | 13.97858 | 1.11576 |
| 6 | 500mm | open | 15.24324 | 14.27338 | 0.96986 |
| 7 | 560mm open | open | 15.18231 | 14.26292 | 0.91939 |
| 8 | open | 100mm | 15.08767 | 14.17513 | 0.91254 |
| 9 | open | 200mm | 15.0557 | 14.15513 | 0.90057 |
| 10 | open | 300 mm | 15.02711 | 14.15363 | 0.87348 |
| 11 | open | 400mm | 15.03283 | 14.23974 | 0.79309 |
| 12 | open | 500mm | 15.01238 | 14.40372 | 0.60866 |
| 13 | open | 590mm (closed) | 15.11233 | 15.11233 | 0.00000 |

# Appendix C

## CFD results

### C.1 Middle section: Mesh adaptation

The cross flow velocities, pressure drop and $y^+$ values were calculated and the mesh adapted using the maximum $y^+$ value (figures C.1, C.2 and C.3) for a mass flow rate of 28 kg/s.

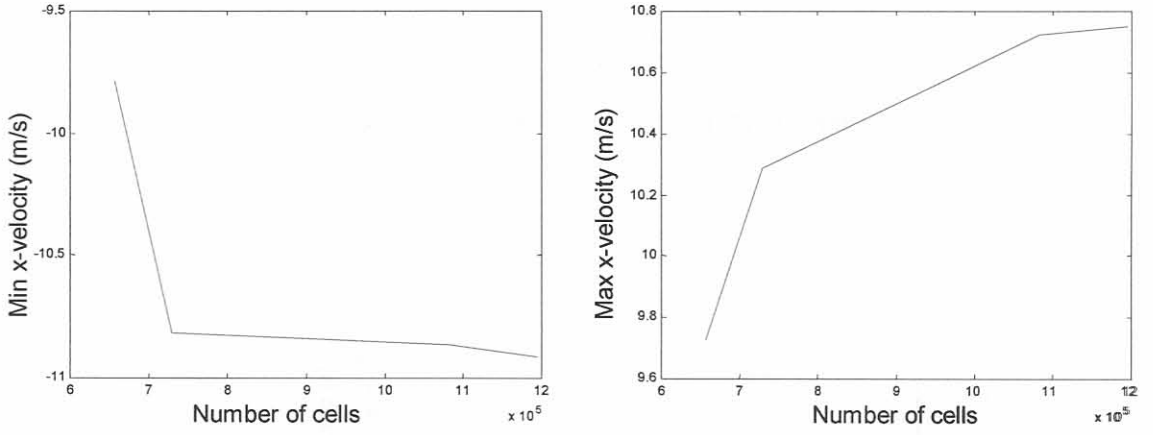


*a) **Minimum** x-velocity* *b) Maximum x-velocity*

*Figure C.1: Minimum and maximum cross-flow velocity in the x-direction*

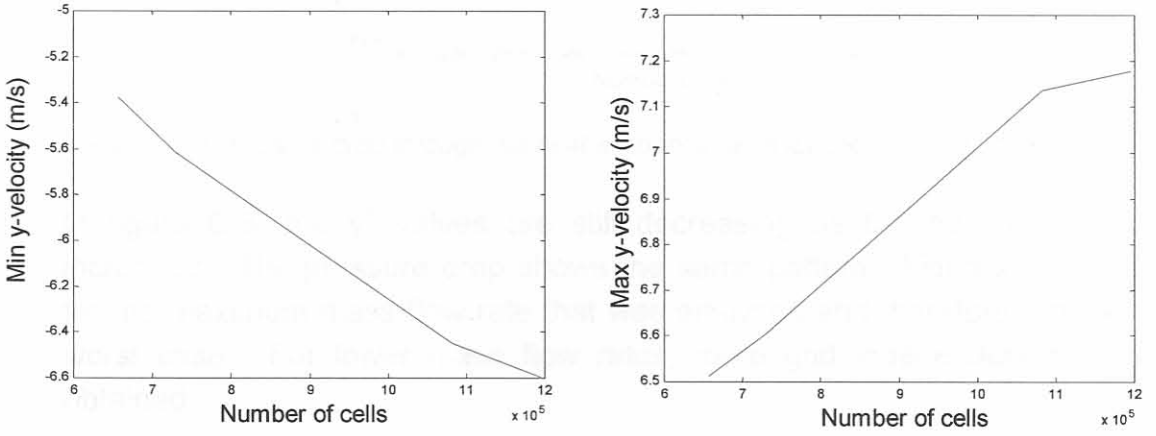


*a) Minimum y-velocity* *b) Maximum y-velocity*

*Figure C.2: Minimum and maximum cross-flow velocity in the y-direction*

Figures C.1 and C.2 show the cross-flow velocities as functions of the number of cells used in the FLUENT analysis. In most cases the velocities started to converge. Due to limitation in computational power, the mesh could not be adapted further.

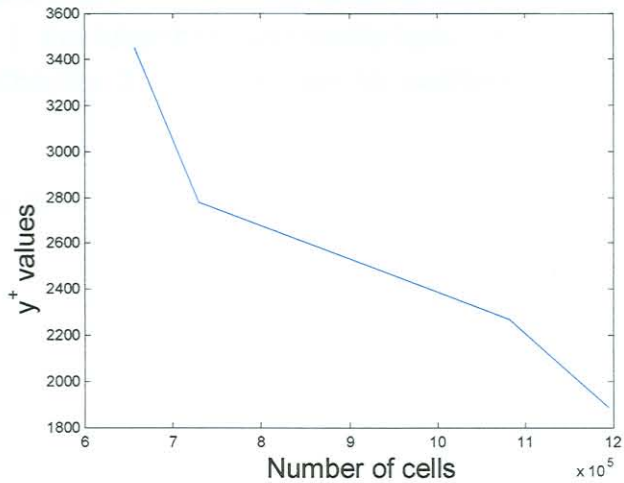


*Figure C.3: $y^+$ values as a function of the number of cells used*

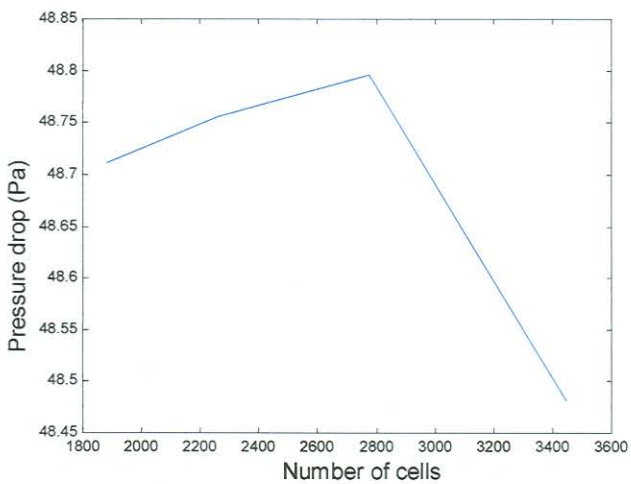


*Figure C.4 Pressure drop through the heat exchanger as a function of the number of cells used*

In figure C.3, the $y^+$ values are still decreasing as the number of cells are increased. The pressure drop shows the same pattern. Figures C.1 to C.4 are for the maximum mass flow rate that was analysed and therefore represents the worst case. For lower mass flow rates, more grid independent results were obtained.

## C.2 Middle section: Average cross-flow velocity magnitude equations

The average cross-flow velocity between the baffles at different distances from the centre of the heat exchanger, was calculated as described in Chapter 3 (sections 3.2.2 and 3.3.1). The magnitude of the cross-flow velocities between baffle type 3 and 1, the tubesheet and baffle type 1 and between baffle type 1 and 2, are given in Chapter 3. The remaining sections of the heat exchanger are given below.

### C.2.1 Baffle type 1 and 2

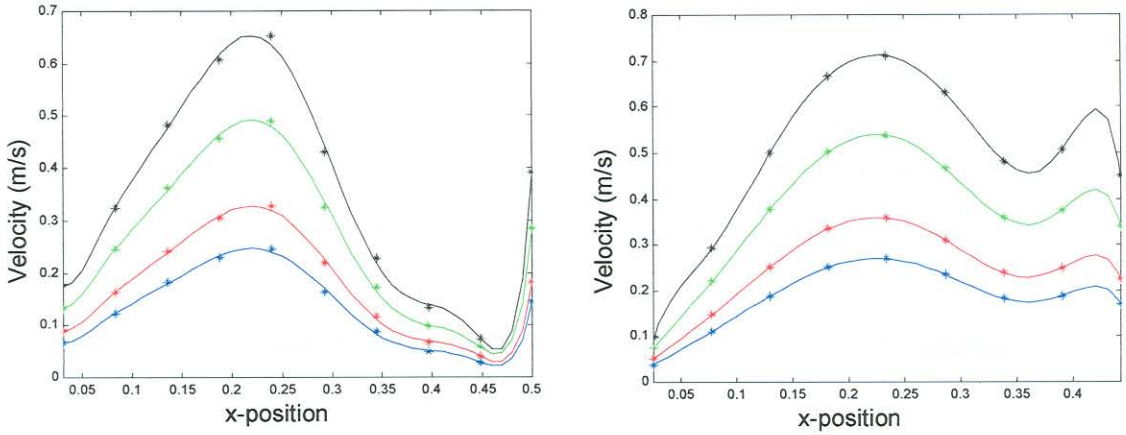


*a) Bottom section* *b) Top section*

*Figure C.5: Velocity magnitude as a function of the x position (blue – 6 kg/s, red – 8kg/s, green – 12kg/s and black – 16 kg/s)*

$$v_{bottom} = -397056\frac{\dot{m}}{4}x^8 + 600518\frac{\dot{m}}{4}x^7 - 376220\frac{\dot{m}}{4}x^6 + 130084\frac{\dot{m}}{4}x^5 - 27282.5\frac{\dot{m}}{4}x^4 + 3320.25\frac{\dot{m}}{4}x^3 - 209.832\frac{\dot{m}}{4}x^2 + 15.3587\frac{\dot{m}}{4}x^1 - 0.061492 \quad \text{C.1}$$

$$v_{top} = 10028.2\frac{\dot{m}}{4}x^8 - 19720.4\frac{\dot{m}}{4}x^7 + 15798.1\frac{\dot{m}}{4}x^6 - 6642.2\frac{\dot{m}}{4}x^5 + 1583.12\frac{\dot{m}}{4}x^4 - 217.95\frac{\dot{m}}{4}x^3 + 16.8099\frac{\dot{m}}{4}x^2 - 0.58031\frac{\dot{m}}{4}x^1 + 0.011452 \quad \text{C.2}$$

### C.2.2 Baffle type 2 and 3

$$v_{bottom} = -196647\frac{\dot{m}}{4}x^8 + 412463\frac{\dot{m}}{4}x^7 - 354926\frac{\dot{m}}{4}x^6 + 161633\frac{\dot{m}}{4}x^5 - 41961\frac{\dot{m}}{4}x^4 + 6256.0\frac{\dot{m}}{4}x^3 - 518.73\frac{\dot{m}}{4}x^2 + 22.2633\frac{\dot{m}}{4}x^1 - 0.31878 \quad \text{C.3}$$

$$v_{top} = 4229.38\frac{\dot{m}}{4}x^6 - 6359.13\frac{\dot{m}}{4}x^5 + 3617.4\frac{\dot{m}}{4}x^4 - 956.5614\frac{\dot{m}}{4}x^3 + 114.8707\frac{\dot{m}}{4}x^2 - 4.972265\frac{\dot{m}}{4}x^1 + 0.096557 \quad \text{C.4}$$

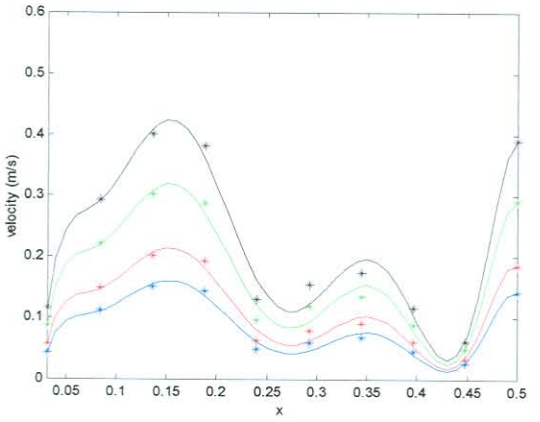


a) Bottom section

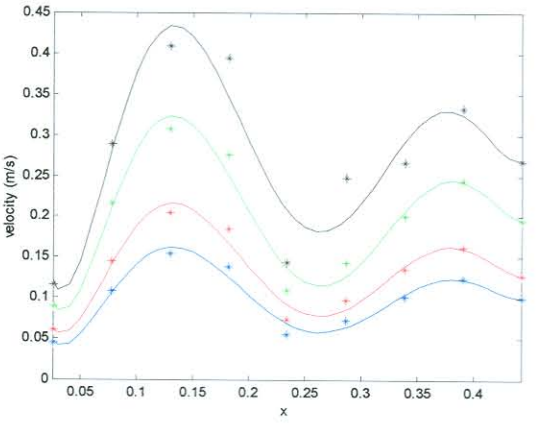


b) Top section

*Figure C.6: Velocity magnitude as a function of the x position (blue – 6 kg/s, red – 8kg/s, green – 12kg/s and black – 16 kg/s)*

## C.3 Inlet section: Average cross-flow velocity magnitude equations

### C.3.2 Baffle type 2 and 3

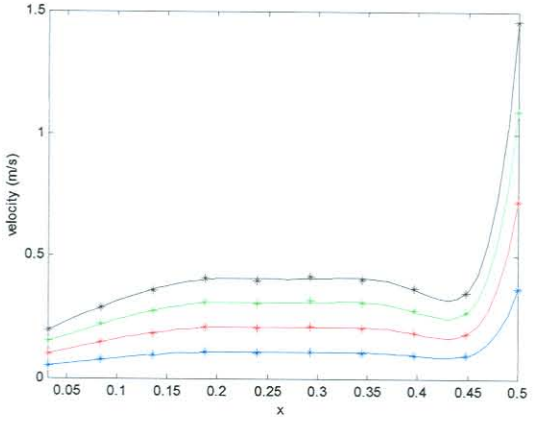


a) Bottom section

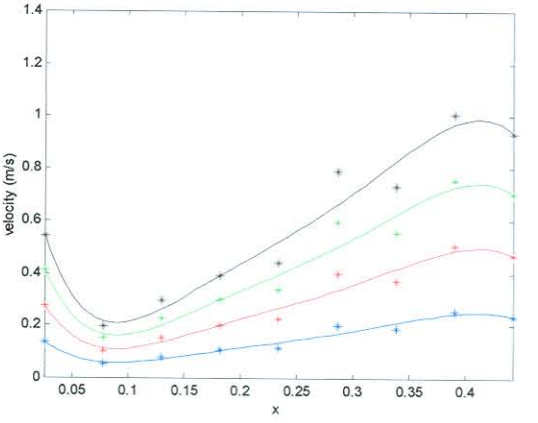


b) Top section

*Figure C.7: Velocity magnitude as a function of the x position (blue – 6 kg/s, red – 8kg/s, green – 12kg/s and black – 16 kg/s)*

$$v_{bottom} = 9058.91\frac{\dot{m}}{2}x^8 - 13489.6\frac{\dot{m}}{2}x^7 + 7792.74\frac{\dot{m}}{2}x^6 - 2200.15\frac{\dot{m}}{2}x^5 + 317.73\frac{\dot{m}}{2}x^4 - 23.209\frac{\dot{m}}{2}x^3 + 0.44214\frac{\dot{m}}{2}x^2 - 0.25877\frac{\dot{m}}{2}x^1 + 0.016375 \quad \text{C.5}$$

$$v_{top} = 244.577\frac{\dot{m}}{2}x^6 - 555.813\frac{\dot{m}}{2}x^5 + 447.075\frac{\dot{m}}{2}x^4 - 172.079\frac{\dot{m}}{2}x^3 + 34.402\frac{\dot{m}}{2}x^2 - 3.1311\frac{\dot{m}}{2}x^1 + 0.12839 \qquad \text{C.6}$$

# Appendix D

## Measuring positions

### D.1 Measuring positions

### D.1.1 Strain gauge positions

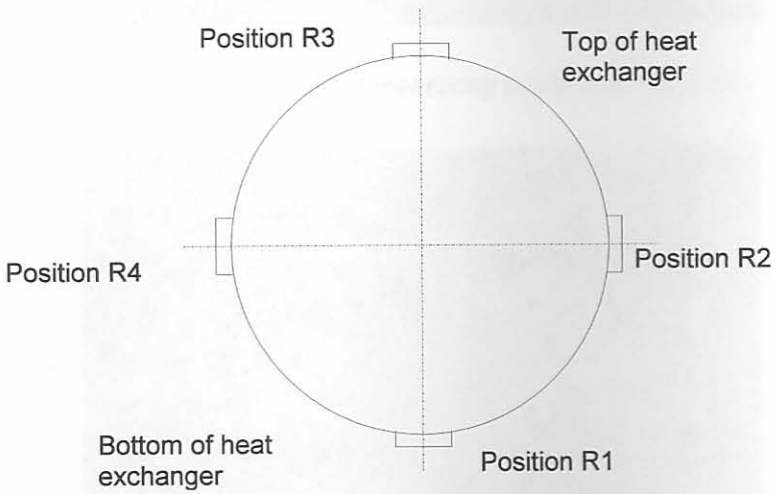


*Figure D.1: Strain gauge positions*

Measurements at R1 to R4 were taken with KFW-5-120-C1-16L5M2R strain gauges. The strain gauges at position R3 gave some problems and no measurements were taken at that position. Variation in strain was measured at the remaining positions

### D.1.2 Support measurement positions

Measurements at B1 to B4 were taken with 2V/g accelerometers.

- B1 measuring acceleration in the negative x-direction
- B2 measuring acceleration in the negative z-direction
- B3 measuring acceleration in the positive y-direction
- B4 measuring acceleration in the negative x-direction


*Figure D.2: Support measuring positions B1 and B2*


*Figure D.3: Supports measuring positions B3 and B4*

### D.1.3 Shell measurement positions

Measurements taken at A1, A3 and A4 were taken with 500mV/g accelerometers. The measurements as A2 were taken with a 100mV/g accelerometer.

- A1 measuring acceleration in the negative y-direction
- A2 and A3 measuring acceleration in the negative x-direction
- A4 measuring acceleration in the positive y-direction

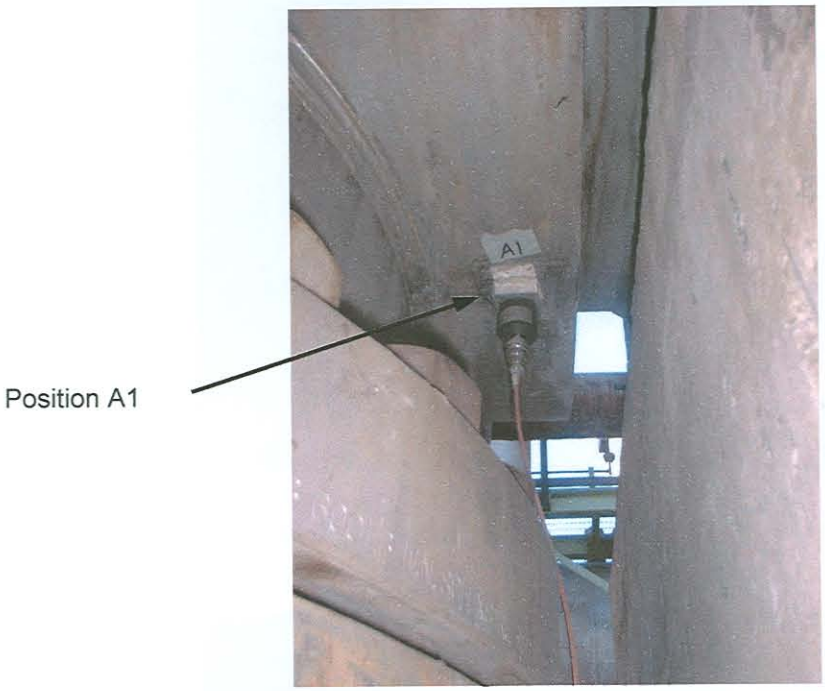


*Figure D.4: Shell measuring position A1 (at outlet)*

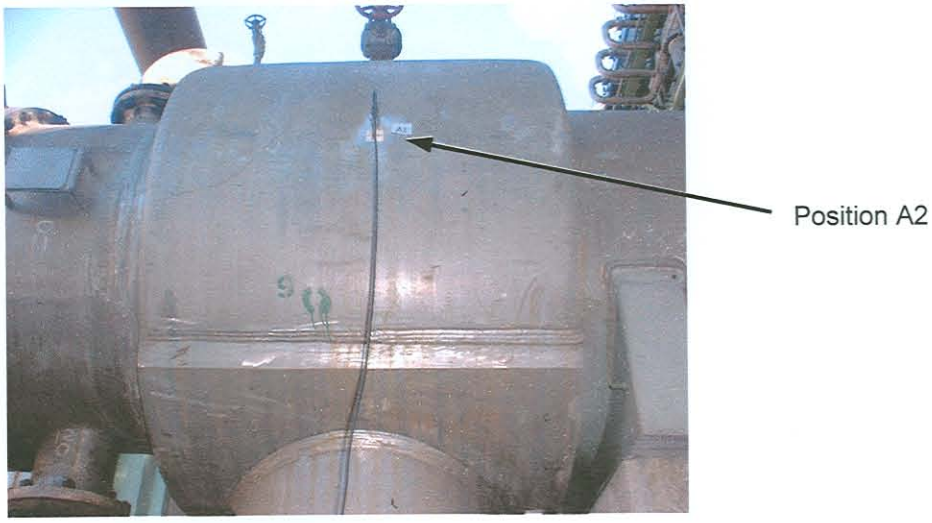


*Figure D.5: Shell measuring position (A2) 90° from outlet*

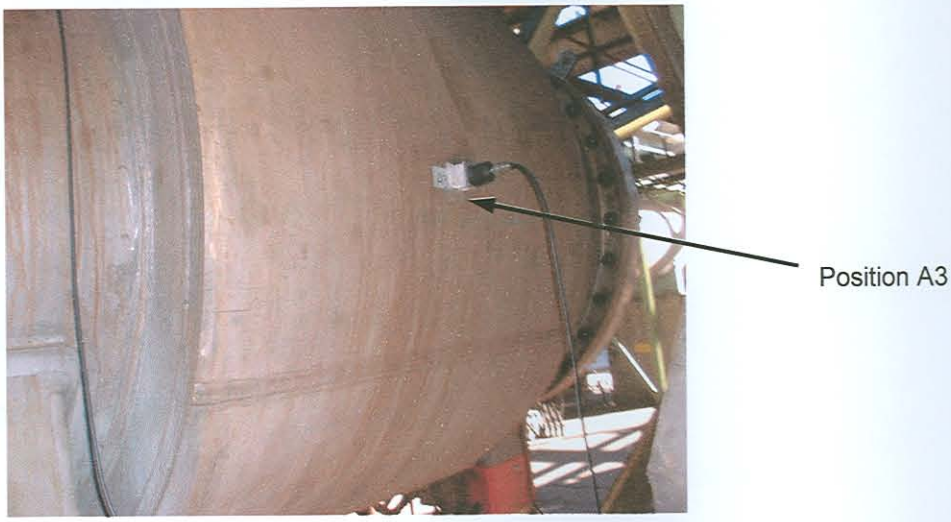


*Figure D.6: Shell measuring position (A3) 90° from outlet*


*Figure D.7: Measuring position A1 at inlet*

# Appendix E

## Experimental results

### E.1 Experimental results

### E.1.1 Strain gauge measurements

**Position R1**

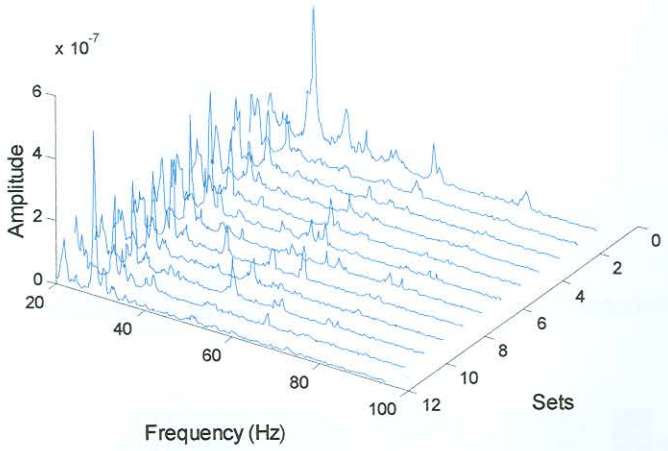


*Figure E.1: Waterfall plot for strain gauge measurements*

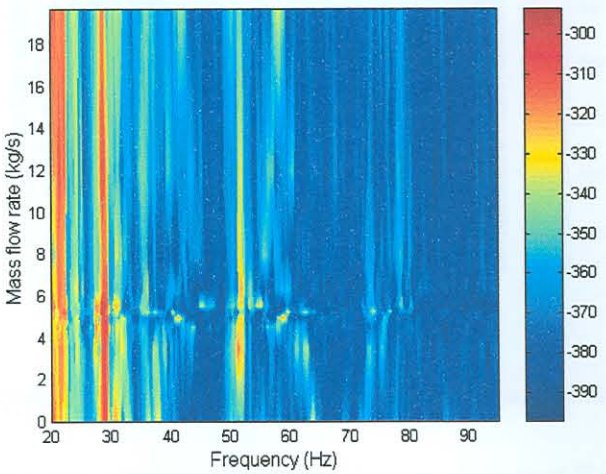


*Figure E.2: Contour plot for strain gauge measurements*

Increased strain amplitudes are visible at 28.5 Hz and a smaller peak 27.5 Hz, as well as at 52 Hz (figures E.1 and E.2). The 27.5 and 28.5 Hz peaks are similar to the predicted HTRI and FEM calculated values of 28.56 Hz and 27.76 Hz respectively.

## Position R2

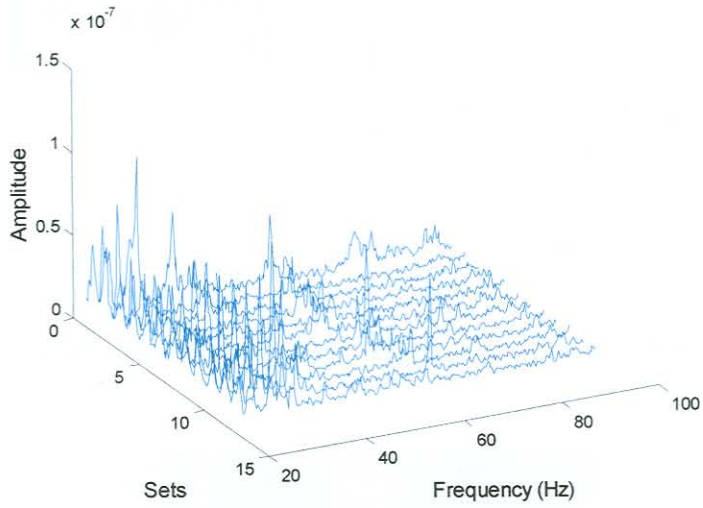


*Figure E.3: Waterfall plot for strain gauge measurements*

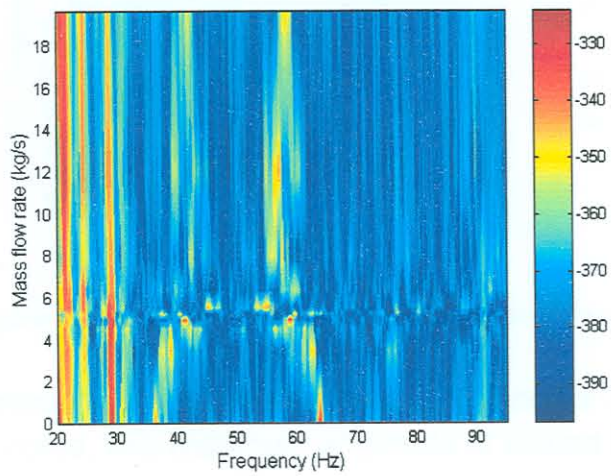


*Figure E.4: Contour plot for strain gauge measurements*

Figures E.3 and E.4 show similar results as figures E.1 and E.2, with an increase in strain amplitude at 29 Hz. This value is also similar to the predicted values.

## Position R4

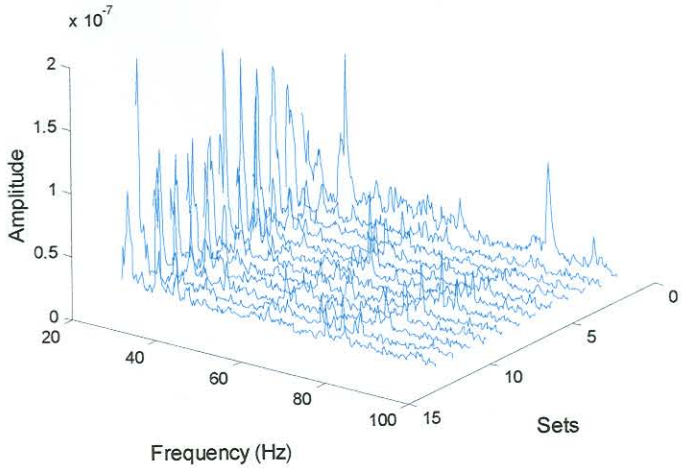


*Figure E.5: Waterfall plot for strain gauge measurements*

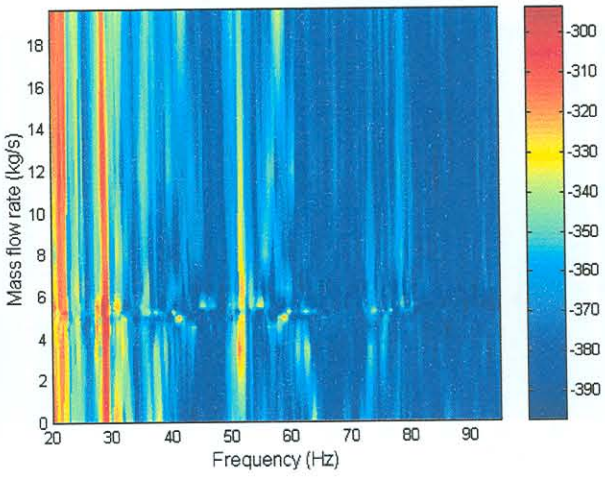


*Figure E.6: Contour plot for strain gauge measurements*

In figure E.6 an increase in strain amplitude at a frequency of 28.7 Hz through the flow ranges can be noted, with maximum amplitude at around 6 kg/s.

The strain gauge measurements at all three positions indicate vibration at a frequency between 28 Hz and 29 Hz. This corresponds well to the predicted values.

## E.1.2 Support measurements

### Position B1

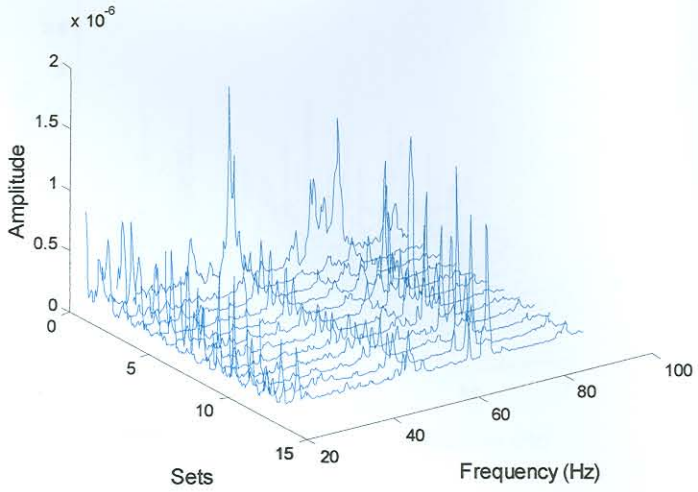


*Figure E.7: Waterfall plot of support measurements*

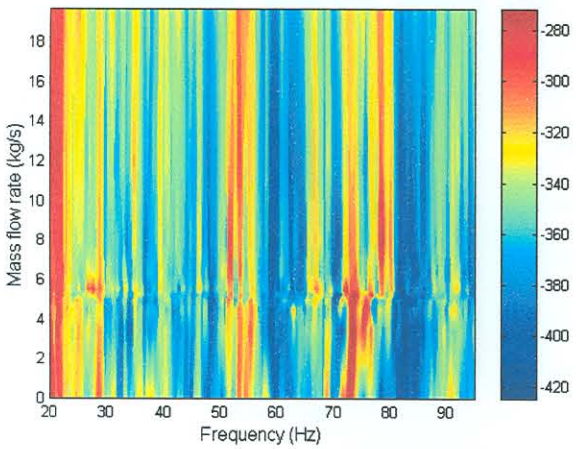


*Figure E.8: a) Contour plot of support measurements*

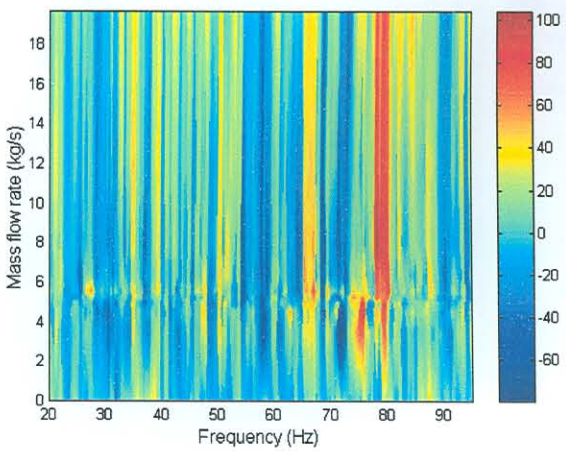


*b) Contour plot of difference in support measurements*

In figures E.7 and E.8a), a frequency at 28.5 Hz is visible up until 16 kg/s, after which it starts to decrease in amplitude. Other noticeable frequencies are at 52 Hz and 80 Hz. In figure E.15b) an increase in amplitude at a mass flow rate of 6 kg/s and 27.5 Hz is observed, as well as an increase in amplitude at 65 Hz between a mass flow rate of 6kg/s and 16 kg/s. Again there is a good correlation between the measured frequencies of 28.5 Hz and 27.5 Hz, and the predicted values.

## Position B2

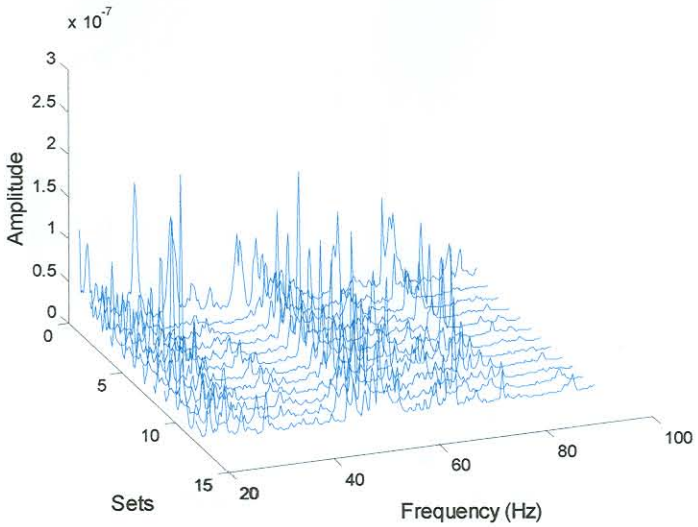


*Figure E.9: Waterfall plot of support measurements*

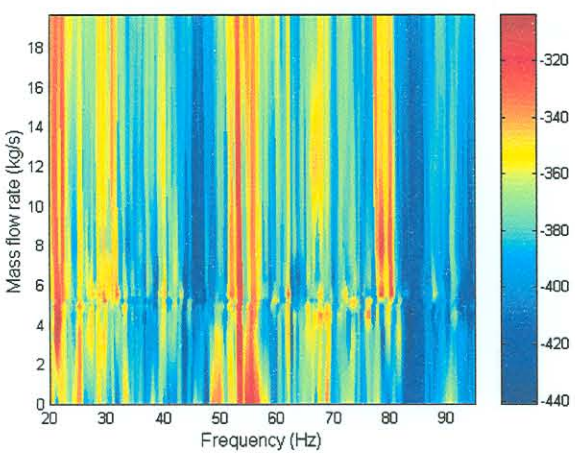


*Figure E.10: a) Contour plot of support measurements*

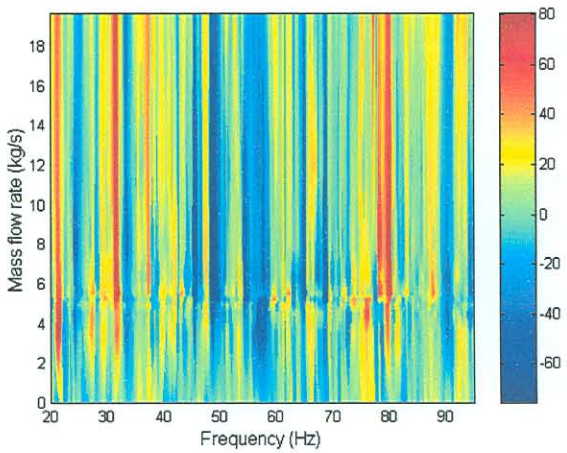


*b) Contour plot of difference in support measurements*

No increase in vibration is observed at the predicted values, there are however an increase in vibration at 53 Hz and 80 Hz (figures E.9 and E.10 a). In figure E.10 b) the non-operational measurements are deducted from the operational measurements. In that figure no frequency band at 53 Hz is observed, this indicates that the vibration was coming from an external source.

## Position B3

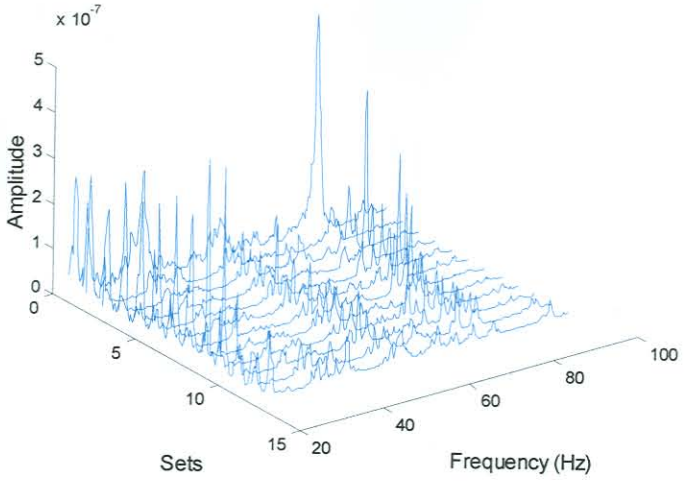


*Figure E.11: Waterfall plot of support measurements*

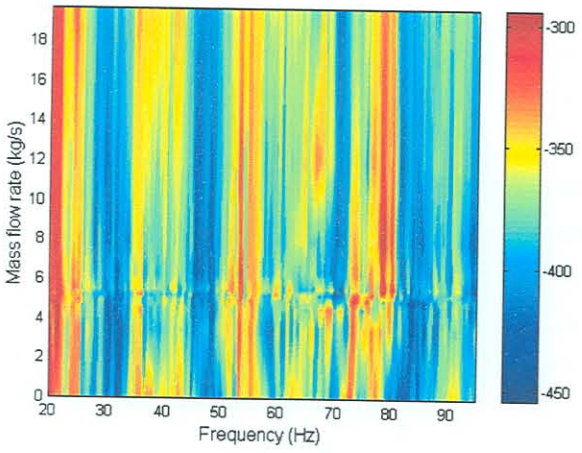


*Figure E.12: a) Contour plot of support measurements*

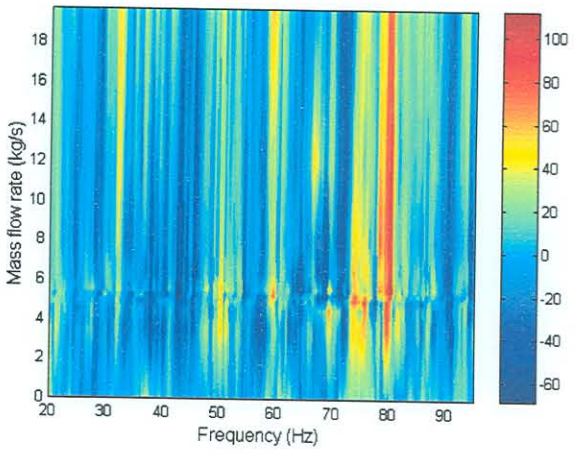


*b) Contour plot of difference in support measurements*

Figure E.12 a) and b) indicates vibration at a frequency of 80 Hz from a mass flow rate of 3 kg/s and upward. Figure E.18 also indicates vibration at a frequency of 25 Hz throughout the mass flow range, as well as frequency band between 35 Hz and 43 Hz, and 53 Hz and 56 Hz.

## Position B4

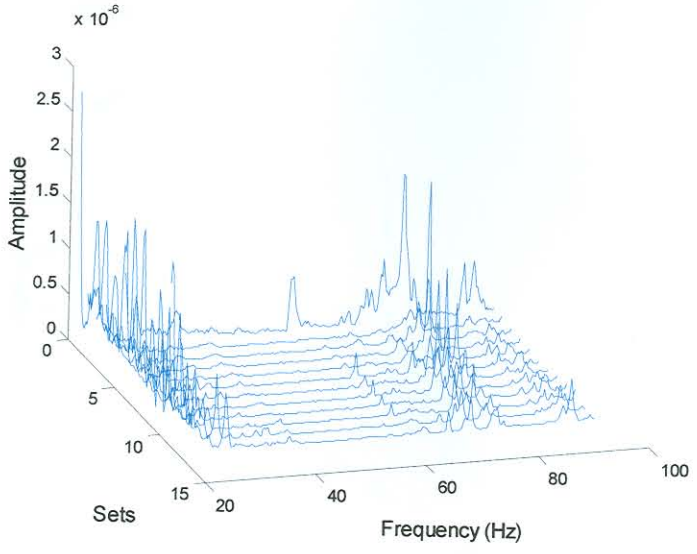


*Figure E.13: Waterfall plot of support measurements*

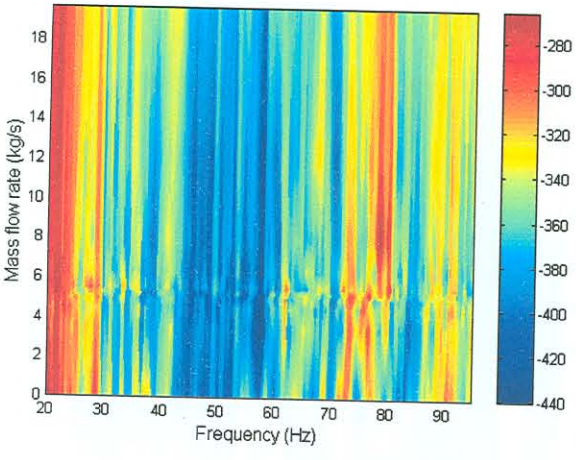


*Figure E.14: a) Contour plot of support measurements*

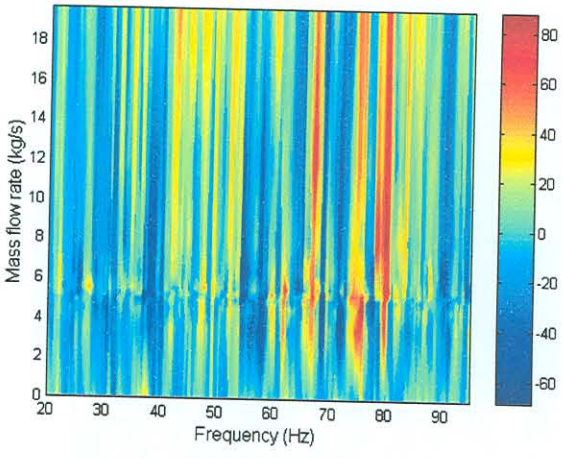


*b) Contour plot of difference in support measurements*

Throughout the flow range, vibration at a frequency of 28.5 Hz, is observed (figures E.13 and E.14 a). In figure E.14 b) a peak at 6 kg/s and 27.5 Hz is also visible. Good correlation between the predicted values from Chapter 2 are again obtained.

### E.1.3 Shell measurements

### Position A1

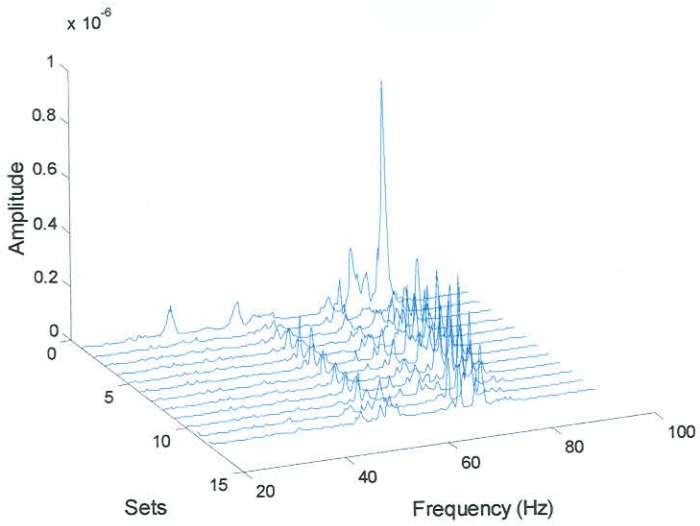


*Figure E.15: Waterfall plot of shell measurements*

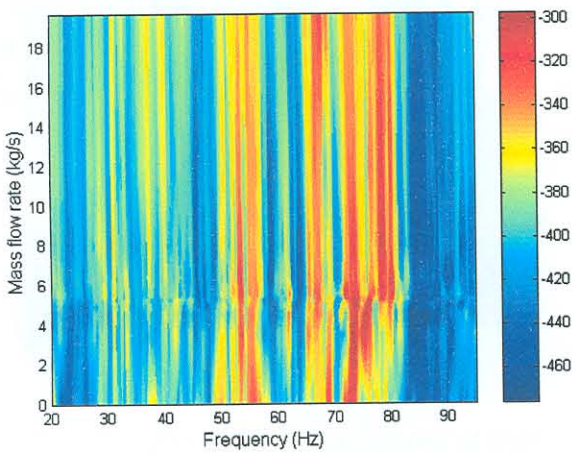


*Figure E.16: a) Contour plot of shell measurements*

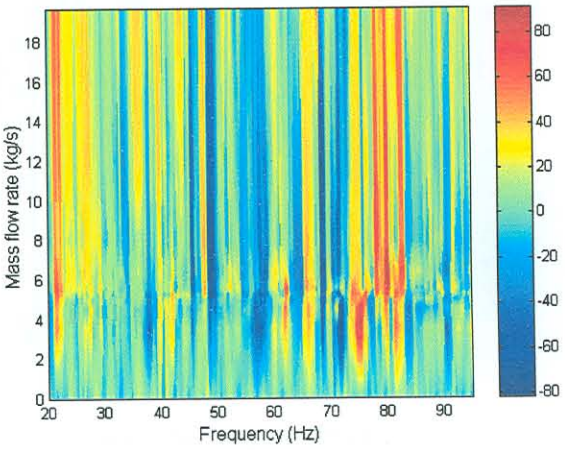


*b) Contour plot of difference in shell measurements*

Frequency band between 50 Hz and 60 Hz, as well as between 70 Hz and 80 Hz are observed (figures. E.15 and E.16 a). No vibration is visible at the expected frequencies.

## Position A2

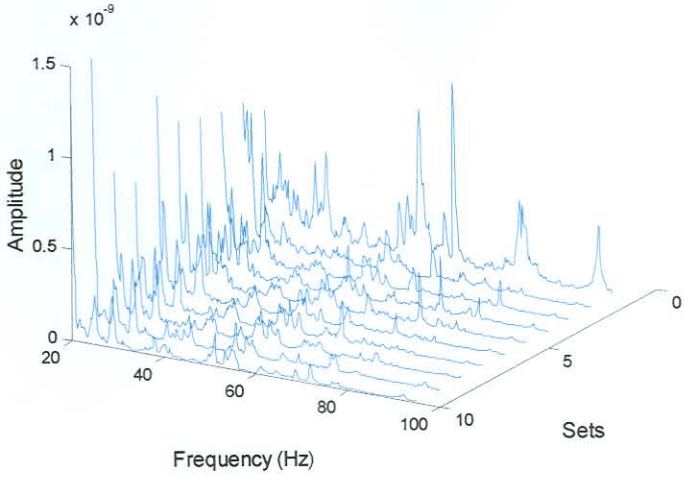


*Figure E.17: Waterfall plot of shell measurements*

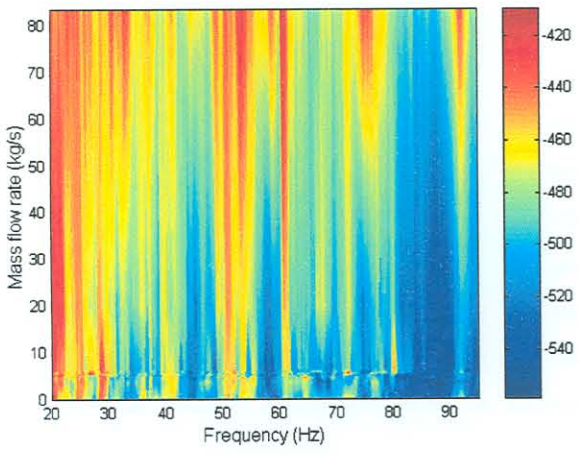


*Figure E.18: a) Contour plot of shell measurements*

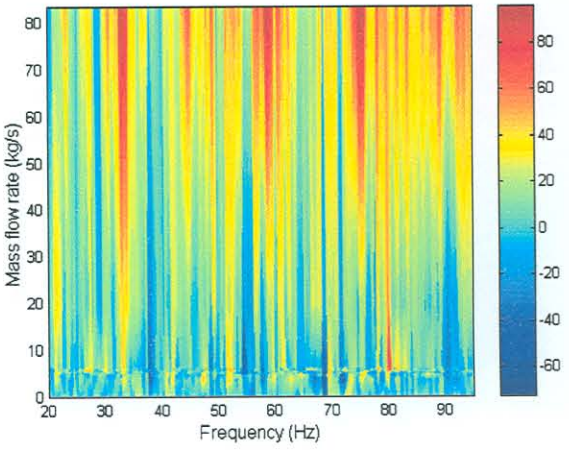


*b) Contour plot of difference in shell measurements*

At 24 Hz and 28Hz, increase in acceleration was recorded throughout the mass flow range. At a frequency of 32 Hz, an increase in amplitude is noted from a mass flow range of about 5 kg/s and upwards (figures E.17 and E.18).

## Position A3

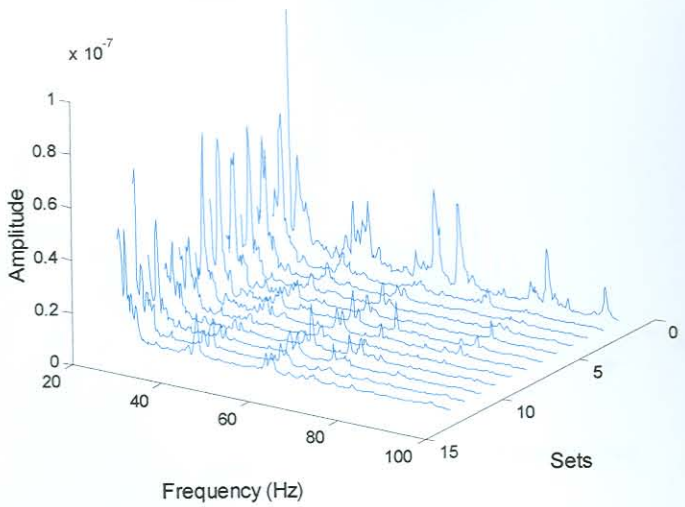


*Figure E.19: Waterfall plot of shell measurements*

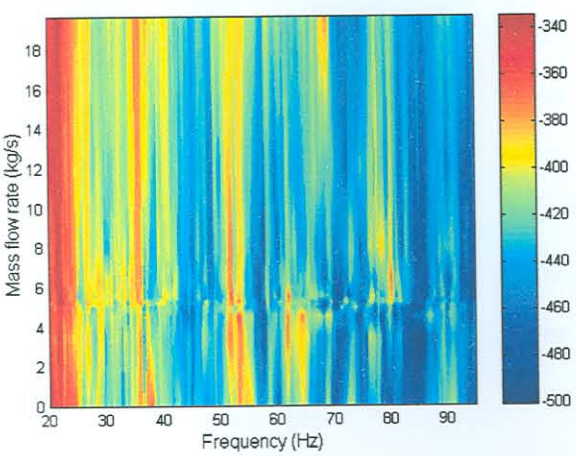


*Figure E.20: a) Contour plot of shell measurements*

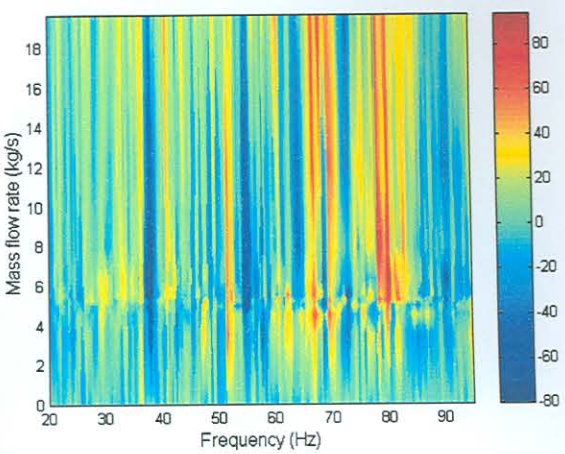


*b) Contour plot of difference in shell measurements*

In figure E.20 a), vibration at a frequency of 36 Hz throughout the flow range was measured. The amplitude of vibration at this frequency, increased as the mass flow rate was increased. (Also see figure E. 19)

## Position A4

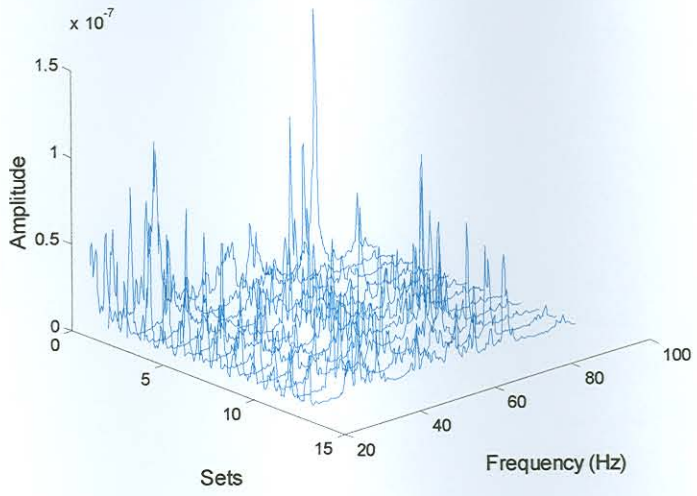


*Figure E.21: Waterfall plot of shell measurements*

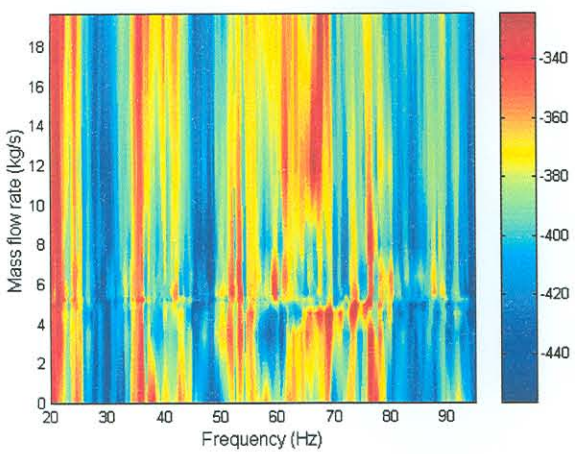


*Figure E.22: a) Contour plot of shell measurements*

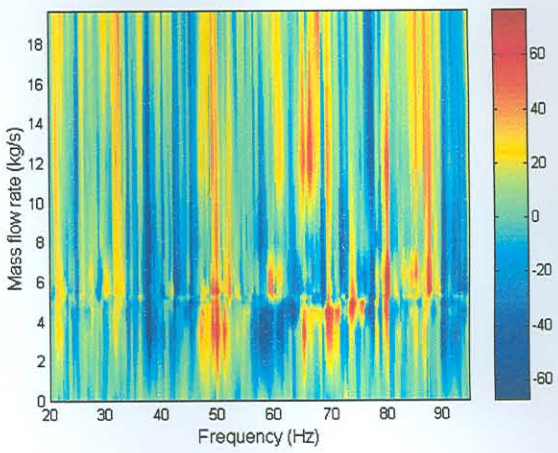


*b) Contour plot of difference in shell measurements*

Vibration at a frequency of 36 Hz is again observed in figure E.22 a). Figure E.22 b) also indicates an increase in vibration at this frequency from a mass flow rate of 4 kg/s and upwards. An increase in acceleration was also measured at 25 Hz (figure E.21).